A Regenerative Cascaded Multilevel Converter Adopting Active Front Ends Only in Part of Cells

Jinwu Gong, Lan Xiong, Fei Liu, and Xiaoming Zha, *Member, IEEE*

***Abstract*—This paper studies a regenerative cascaded multilevel converter that substitutes active front ends for the diode-based front ends only in part of cells, and proposes a power tracking control strategy that does not need any motor parameters. During the induction motor's deceleration, by controlling the two kinds of cells' output voltages according to the motor's power factor angle, the converter makes the motor-generated energy wholly collected by regenerative cells; thus, other cells' dc-link voltages remain stable. Regeneration limitation is analyzed. The simulation results of a 6-kV six-cell cascaded converter and experiments on a laboratory cascaded converter verify that the converter can transfer the motor power back to the grid and allows the motor to decelerate more quickly. Moreover, the control strategy is suitable for the drive systems whose regenerated power cannot be estimated or is varying.**

***Index Terms*—Active front end (AFE), cascaded multilevel converter, regeneration limitation, regenerative topology.**

I. Introduction

[1]–[7]. This kind of a converter has many advantages, such as adaptability to higher voltage level, relatively high power quality both at the grid side and the motor side, and modularity. Currently, control methods used by a CHB multilevel converter are mainly developed on the basis of two control strategies, i.e., V/f control and field-oriented control (FOC) [7]. FOC has much better speed regulation performance than V/f control, but it requires elaborate motor parameters, and its performance relies on the accuracy of parameters. Therefore, V/f control is still widely used as a simple and universal method for fan and pump drives powered by a CHB multilevel converter, which do not need rapid speed regulation. Some scholars have made effort on improving the performance of V/f control [8]–[14].

Manuscript received November 27, 2013; revised March 16, 2014 and July 21, 2014; accepted September 7, 2014. Date of publication September 24, 2014; date of current version March 17, 2015. Paper 2013-IPCC-0965.R2, presented at the 2013 IEEE Energy Conversion Congress and Exposition, Denver, CO, USA, September 16–20, and approved for publication in the IEEE Transactions on Industry Applications by the Industrial Power Converter Committee of the IEEE Industry Applications Society. This work was supported in part by the National Natural Science Foundation of China under Project 51107091 and Project 51307126. *(Corresponding author: Lan Xiong.)*

J. Gong, F. Liu, and X. Zha are with the School of Electrical Engineering, Wuhan University, Wuhan 430072, China (e-mail: gtmobile@foxmail.com; lf_dyj@whu.edu.cn; xmzha@whu.edu.cn).

L. Xiong is with the School of Electrical and Electronic Engineering, Hubei University of Technology, Wuhan 430068, China (e-mail: xusbl@hotmail.com).

Color versions of one or more of the figures in this paper are available online at http://ieeexplore.ieee.org.

Digital Object Identifier 10.1109/TIA.2014.2360014

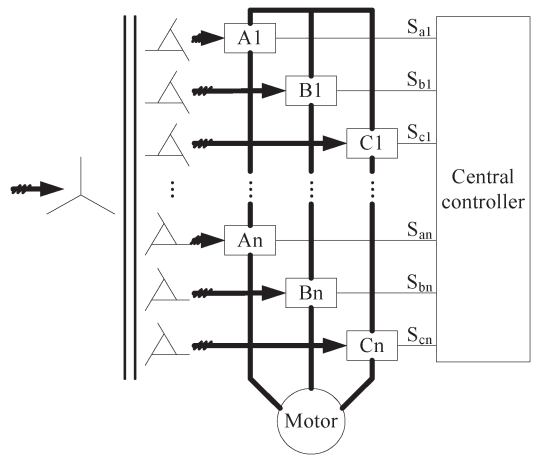

Fig. 1. Topology of the CHB multilevel converter.

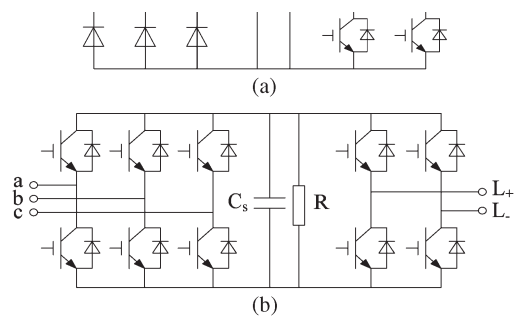

Fig. 2. Cell topologies. (a) Nonregenerative with diode-based rectifier. (b) Regenerative with three-phase PWM rectifier.

Conventional CHB multilevel converter topology is shown in Fig. 1. A phase-shift transformer powers all the cascaded cells. Each cell, as shown in Fig. 2(a), is composed of a three-phase diode-based rectifier, a dc-link capacitor, a parallel resistor, and an H-bridge inverter. This topology is unable to deliver the motor's energy to the grid. When the motor decelerates with a relatively rapid speed, the motor runs in generating mode, and the motor energy's accumulating on the dc-link capacitors can damage the converter. Therefore, the deceleration time of big fans is always much longer than acceleration time.

An insulated-gate bipolar transistor (IGBT)-based active front end (AFE), as shown in Fig. 2(b), has been proposed to

replace the diode-based rectifier in each cell [15]–[18]. This is effective but greatly increases the costs on power devices, and each cell needs extra voltage and current measurement circuits for rectifier control, leading to higher cost and control complexity. A single-phase H-bridge and a half-bridge are also suggested as the AFE [19]–[23]. These approaches partly reduce the costs on power devices and the input transformers but will result in larger ripples in dc-link voltage, and the converter is vulnerable to grid-side voltage imbalance. Moreover, in a cell with a single-phase half-bridge as AFE [20], [23], the load current flows through the dc capacitors, which will shorten the capacitors' life. A scheme with a special regenerative cell connected between the neutral points of the inverter and the motor is explored in [24]. It needs an additional reactor and depends on a relatively high zero-sequence voltage that may impair the motor's insulation and bearings.

A topology of cascaded multilevel converter that only replaces diode-based rectifiers with AFE in part of cells is proposed in [25]. It allows bidirectional power flow with lower cost than the CHB converter in which each cell has an AFE; thus, the central controller becomes less complex. This reduction of power devices and control circuits will also bring less probability of failure. A control scheme based on FOC is suggested in [25]. However, the converter's input transformer and grid-side power quality is not discussed.

This paper studies this topology and presents the structure

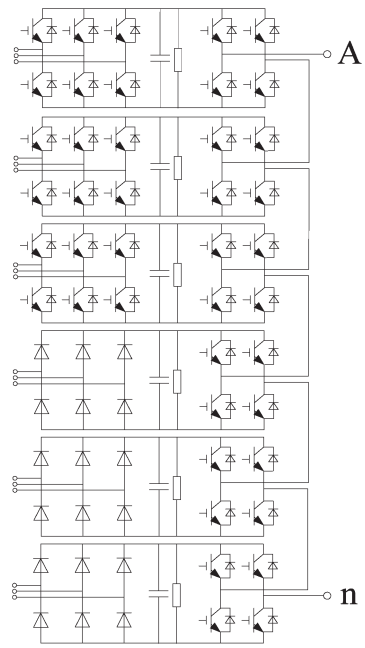

Fig. 3. Per-phase topology of a 6-kV cascaded multilevel converter with three regenerative cells.

current measuring circuits and the switching loss is also higher. Therefore, there is a tradeoff between the performance and cost

developed in this paper for the drive systems whose regenerated power is unknown or varies due to the load, and this method does not need any motor parameter. For the cases in which regenerated power can be estimated, the converter can adopt an open-loop control method that has been presented in [26]. Experiments on a laboratory drive system were conducted to verify the principal of the converter and the feasibility of the control strategy.

II. Topology and Comparison in Cost

In the converter, the diode-based rectifiers in part of the cascaded cells are replaced by IGBT-based rectifiers. Cells with IGBT-based rectifier and diode-based rectifier are called "regenerative" cell and "ordinary" cell, respectively. Regenerative cells work as the channel for energy to flow from the motor to the grid. Thus, the converter has the ability of regenerating. As an example, the per-phase topology of a 6-kV regenerative CHB multilevel converter with three regenerative cells in one phase is shown in Fig. 3.

The number of regenerative cells is variable. The analysis and calculation in Section III will demonstrate that the number of regenerative cells in one phase determines the maximum deceleration speed of the drive system. On one hand, more regenerative cells bring better performance. On the other hand, a regenerative cell costs more than an ordinary cell. It is not only because the device price of an IGBT-based rectifier is higher than a diode-based rectifier, but also because the control of IGBT-based rectifier requires additional voltage and

same with that in a traditional converter, except in the phase degree distribution of the transformer's secondary windings. Because the input currents of regenerative cells and ordinary cells are quite different, the phase shift of the transformer's secondary windings should be rearranged to obtain sinusoidal primary currents and a high power factor. Take the six-cell cascaded converter depicted in Fig. 3 as an example. Because all cells have six-pulse rectifiers, the phase-shift interval is $360^\circ/(6\mathrm{n}) = 10^\circ$ (n is cell number). The original phase-shift angles of the transformer's secondary windings are $\pm 25^\circ$, $\pm 15^\circ$, and $\pm 5^\circ$. The new phase-shift angles for ordinary cells are 20°, 0°, and -20°, and the same angles for regenerative cells.

Under the condition that all cells have the same front ends, more cells involved in the phase-shift disposition will bring better harmonic cancelation effect. Therefore, the harmonic in the proposed converter's input current will be larger than that of a regular converter in which all six secondary windings are equally disposed in phase. However, because part of the converter's input current consists of regenerative cells' input currents that are sinusoidal, the harmonic in the converter's input current will not increase too much.

The rated voltages of the transformer's secondary windings and the dc-link voltages of ordinary cells are the same as before. The dc-link voltages of regenerative cells are set a little bit higher than that of the ordinary cells and are just enough to transfer power to the grid through the transformer. Therefore, the rated voltage of the dc capacitors in all the cells do not need to be raised, and the costs on dc capacitors will not increase.

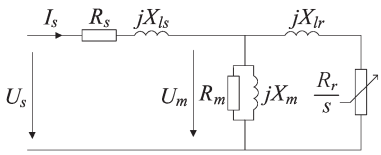

Fig. 4. Induction motor equivalent circuit.

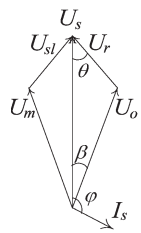

Fig. 5. Induction motor phasor diagram in generating mode.

III. Mechanism of Regeneration and Power Distribution Strategy

When an induction motor is braking or has a load with potential energy, the motor may become a generator under certain condition. This paper is intended to direct the regenerated energy to the grid through regenerative cells.

A. Regeneration Mechanism of Motor's Energy

Fig. 5 shows the motor phasor diagram in generating mode. In the left half of Fig. 5, U_m leads U_s when the motor is in generating mode. U_{sl} is the voltage on stator resistance and stator leakage reactance. The power factor angle φ by which I_s lags U_s exceeds 90°, which means that, at this moment, the converter's output active power is negative, and the energy flows from the motor to the converter.

In the right half of Fig. 5, U_o and U_r represent the output voltage of all the ordinary cells and all the regenerative cells in one phase, respectively. Ordinary cells' output voltage U_o lags U_s by the angle β, and regenerative cells' output voltage U_r leads U_s by the angle θ. Obviously, if U_o is perpendicular to I_s, ordinary cells' output active power will equal zero, and regenerative cells will absorb all the electrical power generated by the motor. Thus, the dc-link voltage of ordinary cells can remain stable during deceleration of the motor.

The control method in [25] requires that U_o and U_r are also in quadrature to each other. It seems reasonable because the regenerative cells only output active power, and the ordinary cells only output reactive power. However, this also puts a restriction on the synthesized output voltage and is less flexible.

B. Power Distribution Strategy

Generally, assuming losses are negligible, the power of a fan or pump system can be expressed as

$$P = \omega_m J \frac{d\omega_m}{dt} + \omega_m \tau_0 \left(\frac{\omega_m}{\omega_{m0}}\right)^2 \tag{1}$$

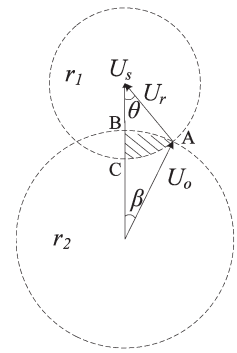

Fig. 6. Variation of U_r, U_o, and angles.

where ω_m, ω_{m0}, J, and τ_0 stand for mechanical angular velocity, the rated mechanical angular velocity, total inertia, and the rated torque of load, respectively [24]. The former part in the right side of (1) represents the mechanical power of the rotating parts, and the latter part represents the load power varying with the mechanical angular velocity. When the motor decelerates, $d\omega_m/dt$ is negative. If the motor decelerates rapidly enough, P becomes negative. Given parameters, the regenerated power P can be estimated by (1), and the converter can adopt an open-loop control method that has been presented in [26]. This paper proposes a control method using power tracking for the cases in which the power P cannot be estimated or varies with the load,

$$P = 3U_s I_s \cos\varphi. \tag{2}$$

When P is negative, β can be calculated by

$$\cos\varphi = \cos\left(\beta + \frac{\pi}{2}\right) = \frac{P}{3U_s I_s} \tag{3}$$

$$\beta = \begin{cases} \arcsin\left(\frac{-P}{3U_s I_s}\right), & P < 0 \\ 0, & P >= 0 \end{cases}. \tag{4}$$

Assume that, in one phase, $U_{\rm dco}$ is the sum of dc-link voltages of all ordinary cells, $U_{\rm dcr}$ is the counterpart of regenerative cells, and all cells have the same modulation ratio m. Then, the relation of the output voltages of these two types of cells is

$$\frac{U_r}{U_o} = \frac{mU_{\rm dcr}/\sqrt{2}}{mU_{\rm dco}/\sqrt{2}} = \frac{U_{\rm dcr}}{U_{\rm dco}}. \tag{5}$$

According to the sine theorem, $U_r/U_o = sin\beta/sin\theta$. Hence, the angle θ by which regenerative cells' output leads the whole converter's output can be calculated by

$$\theta = \arcsin\left(\frac{U_{\rm dco}}{U_{\rm dcr}}\sin\beta\right). \tag{6}$$

According to the cosine theorem

$$\sqrt{2}U_s = \sqrt{(mU_{\rm dco})^2 + (mU_{\rm dcr})^2 - 2m^2 U_{\rm dco}U_{\rm dcr}\cos(\pi - \beta - \theta)}. \tag{7}$$

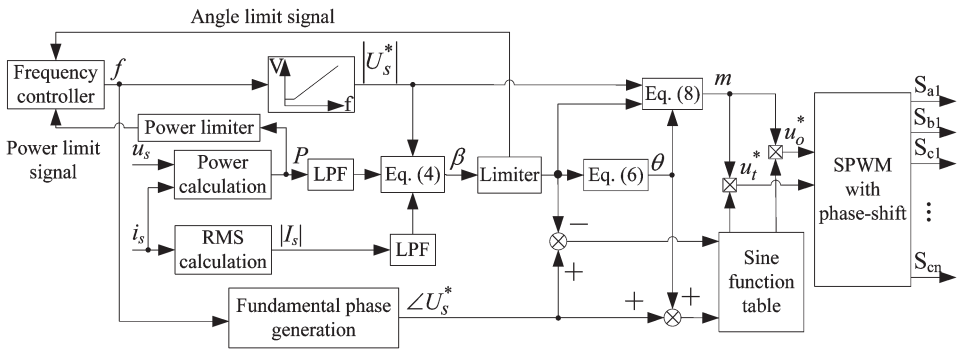

Fig. 7. Proposed control strategy diagram.

Therefore, the modulation ratio of all cells is given by

$$m = \frac{\sqrt{2}U_s}{\sqrt{U_{\rm dco}^2 + U_{\rm dcr}^2 + 2U_{\rm dco}U_{\rm dcr}\cos(\beta+\theta)}}. \quad (8)$$

In V/f control, the converter's output phase voltage U_s and frequency f are known. Moreover, the amplitude of the motor's stator current and active power can be conveniently measured. Therefore, without any motor parameter, all cells' output modulation waves can be calculated online.

Considering that the converter's output phase voltage U_s may deviate from the reference value because of the uncontrolled dc-link voltages of ordinary cells, the modulation ratio of ordinary

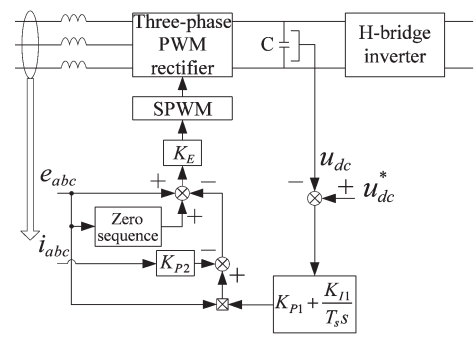

Fig. 8. PWM rectifier control strategy.

$$m_o = m \times \frac{U_{\rm dco}}{\tilde{U}_{\rm dco}} \quad (9)$$

where $\tilde{U}_{\rm dco}$ is the detected value of $U_{\rm dco}$.

Under the same condition, when the regenerated power increases, the power factor angle φ increases, and angle β also should increase to keep the ordinary cells' dc-link voltages stable. On the other hand, from Fig. 5 and (5), it can be seen that the ratio of $U_{\rm dcr}$ to $U_{\rm dco}$ restricts the angle β, which means angle β has an upper limit $\beta_{\rm MAX}$. Therefore, a limiter should be used to keep the angle β under the limit.

Fig. 6 displays the variation of U_r and U_o. When the modulation ratio m varies between 0 and 1, U_r varies in the scope of a circular area r_1, and U_o varies in a circular area r_2. Therefore, the junction point of U_r and U_o can only move in the shaded area ABC. When the junction point of U_r and U_o arrives at point A, the angle β reaches its maximum, and m equals 1. Assume that the converter outputs rated voltage U_{sN}, then the limit $\beta_{\rm MAX}$ is calculated according to the cosine theorem, i.e.,

$$\beta_{\rm MAX} = \arccos\left(\frac{U_{sN}^2 + (U_{\rm dco}/\sqrt{2})^2 - (U_{\rm dcr}/\sqrt{2})^2}{2U_{sN}U_{\rm dco}/\sqrt{2}}\right) = \arccos\left(\frac{2U_{sN}^2 + U_{\rm dco}^2 - U_{\rm dcr}^2}{2\sqrt{2}U_{sN}U_{\rm dco}}\right). \quad (10)$$

When the converter's output voltage is less than U_{sN}, $\beta_{\rm MAX}$ will increase. Therefore, if the angle β keeps less than (10), the converter can adjust its output safely in the whole frequency range. If angle β exceeds the limitation determined by the output voltage U_s and the maximum modulation ratio, then the synthesized output of U_r and U_o will deviate from the reference value U_s, causing the motor to vibrate.

Rotor inertia	172 kg.m^2
Pole pair	2
Number of regenerative cells per phase	3
Number of ordinary cells per phase	3
AC inductor	1 mH
DC-link capacitance	10000 uF
DC-link resistor	50 kΩ
DC-link voltage of ordinary cell	976 V
DC-link voltage of regenerative cell	1100 V
Switching frequency of PWM rectifier	10 kHz
Switching frequency of H-bridge inverter	600 Hz

Larger $\beta_{\rm MAX}$ demands a larger ratio of the sum of all regenerative cells' dc-link voltages to the sum of all ordinary cells' dc-link voltages. When β approaches $\beta_{\rm MAX}$, the limiter warns the frequency controller not to increase the deceleration speed.

Another restriction is the sum of the regenerative cells' rated power, or the rated input current of the regenerative cells, particularly when the number of regenerative cells is relatively small. Sometimes the motor-generated power may exceed the regenerative cells' capacity before the angle β approaches $\beta_{\rm MAX}$.

Under these two restrictions, the converter can automatically decelerate with a relatively rapid speed. The algorithm is summarized in Fig. 7.

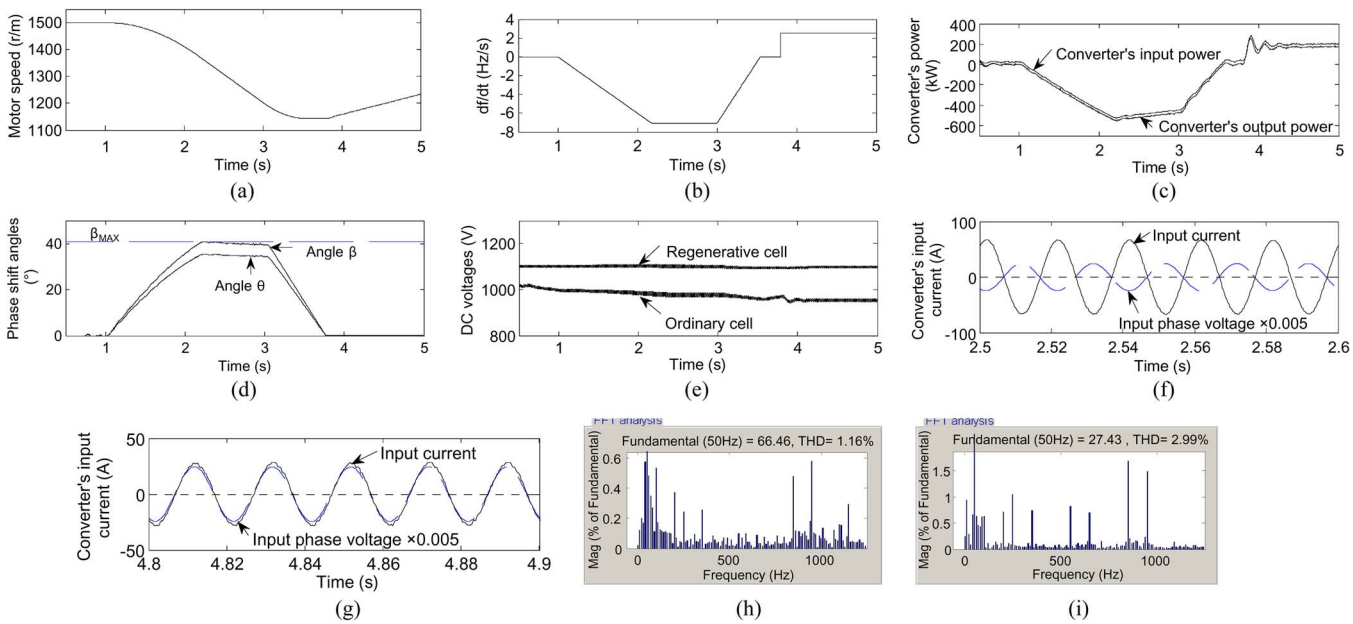

Fig. 9. Simulation results of the proposed regenerative CHB converter. (a) Motor rotation speed. (b) Frequency change rate. (c) Converter's input and output power. (d) Phase shift angles. (e) Cells' dc-link voltages. (f) and (g) Converter's input current during deceleration and acceleration. (h) and (i) Fast Fourier transform analysis of the converter's input current during deceleration and acceleration.

In summary, the boundary conditions needed to guarantee utilization efficiency. In addition to keeping the dc-link voltage

to ordinary cells in one phase, and the regenerated power does not exceed the regenerative cells' capacity. Second, the sum of all cells' dc-link voltages should be properly greater than, not equal to, the value $\sqrt{2}U_s$. Third, the motor should run in steady state to avoid large fluctuations in the motor current and power as far as possible. To suppress the possible oscillation, two low-pass filters are added to the calculation of motor power and current.

On above analysis, it can be seen that, by tracking the motor-generated power and controlling the phase-shift angles of the output voltages of the two kinds of cells, the converter can make the regenerative cells absorb all the motor's power and keep the ordinary cells' dc-link voltages stable during deceleration. If all cells' output phase angles can track the value demanded by the motor's regenerated power, the dc-link voltage of ordinary cells will not rise and are determined by the transformer's output voltage. If the phase-shift angles are bigger than the demanded values, there will be a circulating power among the cells and the transformer. In both cases, ordinary cells' dc-link voltages will keep around the value determined by the transformer's secondary windings.

IV. PWM Rectifier Control

The control scheme of the AFE rectifiers in regenerative cells is depicted in Fig. 8. The outer dc-link voltage loop uses a linear proportional–integral controller. The inner current loop uses a proportional controller and ac voltage feedforward. A zero-sequence component is added to increase the dc voltage

A. Simulation Results

A model of the CHB multilevel converter driving a 6-kV/3100-kW induction motor with no load was established in Matlab/Simulink. The modulation method used in the CHB is carrier-based phase-shift pulsewidth modulation (PS-PWM). The main parameters are summarized in Table I. The dc-link high resistor in the cells represents the parallel resistors connected to series-connected electrolytic capacitors for voltage balance in an actual cell, and will not influence the conclusion because of its high resistance.

Simulation results of the proposed multilevel converter are shown in Fig. 9. According to (10), the upper limit of angle $\beta(\beta_{\mathrm{MAX}})$ by which ordinary cells' output voltage U_o lags U_s, is 40.9° when the converter outputs rated voltage. Therefore, the motor is driven in the following course: 1) the drive system enters steady state in the first second; 2) the deceleration speed $(-df/dt)$ ramps from zero until the angle β approaches the limit β_{MAX}; 3) the deceleration speed keeps at about 7.05 Hz/s until 3 s and then ramps down to zero; and 4) from 3.8 s, the motor accelerates at the speed of 2.5 Hz/s. Fig. 9(a) and (b), respectively, show the motor speed and deceleration speed.

In Fig. 9(c) from 1 to 2.18 s, the motor-generated power rises as the deceleration speed ramps up. While the deceleration speed keeps at 7.05 Hz/s, the motor-generated power slightly decreases as the motor speed decreases. Then, the power decreases as the deceleration speed ramps down to zero. When the deceleration ends, the power turns to positive. Comparing the converter's input and out power, it can be seen that the

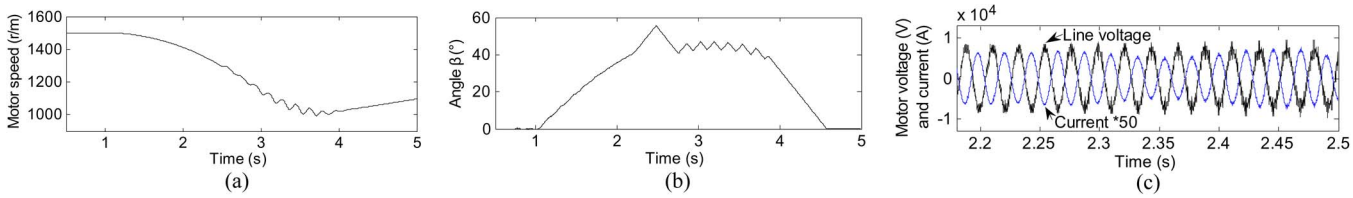

Fig. 10. Simulation results of the regenerative CHB converter when β exceeds the limitation. (a) Motor rotation speed. (b) Phase shift angle. (c) Converter's output line voltage and current.

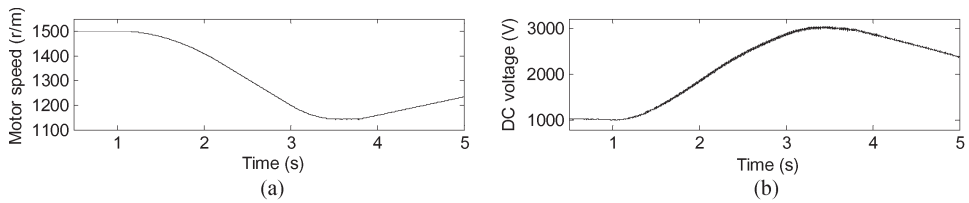

Fig. 11. Simulation results of the conventional CHB multilevel converter. (a) Motor rotation speed. (b) DC-link voltage of cell.

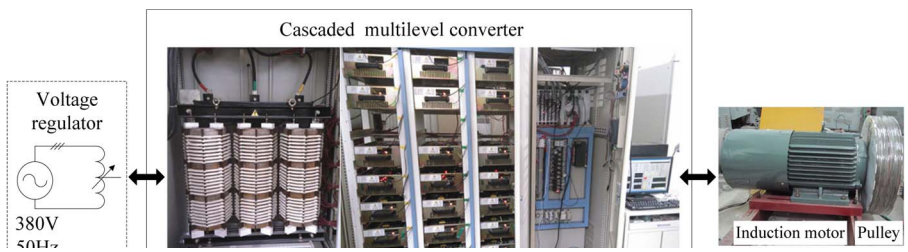

Fig. 12. Experimental platform: Multilevel converter and motors.

motor-generated power mostly flows to the grid while very little part is dissipated in the cells and the phase-shift transformer. Fig. 9(d) shows the angles β and θ. In Fig. 9(e), the ordinary cells' dc-link voltages remain below 1000 V during deceleration, and the regenerative cells' dc-link voltages keep around 1100 V. Fig. 9(f) and (g) shows the converter's input current during deceleration and acceleration, respectively. The total harmonic distortion of the converter's input current is still low.

If the angle limiter does not work, and the deceleration speed ramps up to 10.8 Hz/s, the simulation results are in Fig. 10. When the deceleration speed is about 7.6 Hz/s, and the angle β is about 44°, the converter's output voltage cannot remain stable, and the motor's speed and current begin to vibrate. Because the output voltage at this frequency is smaller than the rated voltage, the real angle limitation is greater than 40.9°.

For comparison, simulation results of a conventional CHB multilevel converter with six ordinary cells cascaded are in Fig. 11. Fig. 11(a) shows the motor mechanical speed. In Fig. 11(b), one of the ordinary cell's dc-link voltage increases to an unacceptable level of 3000 V. Because the cells' input current is zero, the converter's input current almost equals zero and is not depicted.

B. Experimental Results

To verify the principle of the proposed converter and its control strategy, a 380-V induction motor drive system has been built by modifying an existing 10-kV eight-cell cascaded converter. Fig. 12 shows the experimental platform. The key parameters of the motor and the converter are listed in Table II. In order to facilitate the observation of the performance of the drive system, a belt pulley was connected to the motor rotor to increase the rotor inertia J to 0.47 kg · m^2.

TABLE II
PARAMETERS OF MOTOR AND CONVERTER

Motor	
Rated frequency	50 Hz
Rated power	7.5 kW
Rated voltage	380V
Rated current	15 A
Rotor inertia	0.051 kg.m^2
Pole pair	2
Converter	
Number of regenerative cells per phase	1
Number of ordinary cells per phase	4
DC-link capacitance in ordinary cell	3000 μF
DC-link capacitance in regenerative cell	3000 μF
DC-link resistor	30 kΩ
Inductance of PWM rectifier filter	1 mH
Capacitance of PWM rectifier filter	0.5 μF
Rated current of phase shift transformer's secondary windings	4.24 A
Switching frequency of PWM rectifier	6 kHz
Switching frequency of H-bridge inverter	600 Hz

Four ordinary cells and one regenerative cell are cascaded in one phase. Each regenerative cell is composed of a PWM rectifier and an H-bridge inverter whose dc-link bars are connected

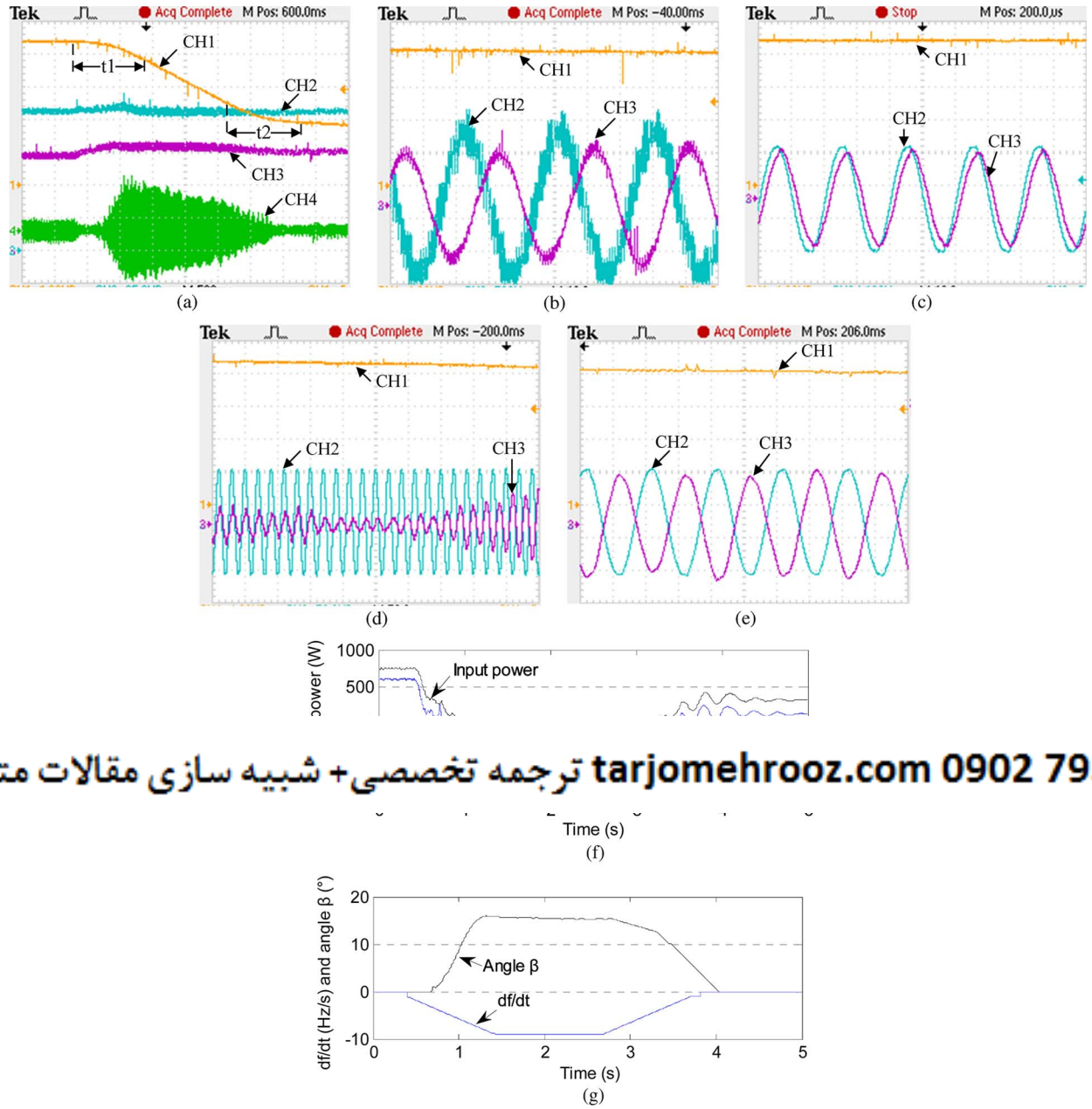

Fig. 13. Experimental results of the proposed converter with constant deceleration speed. (a) Deceleration process: 38–15 Hz, deceleration speed is 9 Hz/s. CH1, motor speed, 250 r/min/div; CH2, regenerative cell's dc voltage, 25 V/div; CH3, ordinary cell's dc voltage, 25 V/div; CH4, regenerative cell's input current, 5 A/div; time, 500 ms/div. (b) Converter's output voltage and current in deceleration process. CH1, motor speed, 250 r/min/div; CH2, converter's output line voltage, 200 V/div; CH3, converter's output current, 10 A/div; time, 10 ms/div. (c) Converter's input current in motoring mode. CH1, motor speed, 250 r/min/div; CH2, converter's input phase voltage, 200 V/div; CH3, converter's input current, 2 A/div; time, 10 ms/div. (d) Change of converter's input power factor at the beginning of deceleration. CH1, motor speed, 250 r/min/div; CH2, converter's input phase voltage, 200 V/div; CH3, converter's input current, 5 A/div; time, 50 ms/div. (e) Converter's input current in regenerating mode. CH1, motor speed, 250 r/min/div; CH2, converter's input phase voltage, 200 V/div; CH3, converter's input current, 5A/div; time, 10 ms/div. (f) Converter's power in deceleration process. (g) Frequency change rate and angle β in deceleration process.

in parallel. To reduce power loss, the original power devices, IGBTs are replaced by MOSFETs (IRFS4227). A capacitor of 0.5 μF is used between the rectifier's inductor and the phase-shift transformer to further reduce the harmonic produced by the PWM rectifier.

The dc-link voltages of ordinary cells and regenerative cells are, respectively, about 80 and 103 V before driving the motor. The dc overvoltage threshold is set at 120 V.

The central controller is composed of a digital signal processor (TMS320F2812) and a field-programmable gate array (EP2C50F484C8). The motor speed, voltages, and currents in the experiment were recorded by a Tektronix oscilloscope TPS2014. Other data, such as the frequency, frequency change rate, phase-shift angles, and the converter's power were recorded by the converter's central controller. The experimental results of a deceleration speed of 9 Hz/s are in Fig. 13.

Fig. 13(a) shows the motor speed, dc-link voltages of an ordinary cell and a regenerative cell, and the input current of the regenerative cell. Before the experiment begins, the converter's output frequency is 38 Hz, and the motor runs in steady state,

and the dc-link voltage of the ordinary cell and the regenerative cell are 74 and 103 V, respectively. First, the converter's deceleration speed ramps from 1 to 9 Hz/s in $t1$(about 1.1 s), then remains at 9 Hz/s in the following 1.2 s, and finally ramps to 1 Hz/s in $t2$(about 1.1 s). The time periods t1 and t2 are indicated in Fig. 13(a). When the deceleration process ends, the frequency stays at 15 Hz. In this process, the dc-link voltages of the ordinary cell and the regenerative cell remain stable.

When the motor begins to decelerate, the ordinary cell's dc-link voltage rises up from 74 to 84 V, and then keeps at 80 V until the motor stops decelerating. This is because, when the converter's output power becomes negative, the angle β by which ordinary cells' output voltage U_o lags U_s has to ramp up from zero to the calculated value. In this transient, ordinary cells absorb part of the motor-generated power. After this transient process, all the ordinary cells' output power equal zero, and their dc-link voltages fall to 80 V. When the motor stops decelerating, ordinary cells output positive power again, and their dc-link voltages fall to 75 V.

According to (10), the limit β_{MAX} is 18.7° when the output is rated voltage and becomes bigger as the frequency goes down. Because, in Fig. 13(a), the regenerative cell's input current rises to 5 A, which is bigger than the rated current of the transformer's secondary windings (4.24 A), and the angle β has not arrive at its limitation, therefore, the experiment platform's maximum regeneration power is limited by the capacity of the

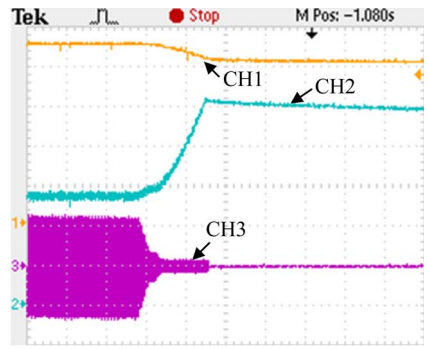

Fig. 14. Experimental results of a traditional converter. CH1, motor speed, 250 r/min/div; CH2, ordinary cell's dc voltage, 25 V/div; CH3, converter's input current, 2 A/div; time, 500 ms/div.

VI. Conclusion

Adopting AFEs only in part of cells makes the converter have limited regeneration capability. This paper has designed the input transformer's structure to obtain good grid-side power quality and presents a power tracking control strategy. The limitations of the drive system's deceleration speed and regenerated power are limited by both the ratio of the sum of all regenerative cells' dc-link voltages to the sum of all ordinary cells' dc-link voltages and the regenerative cell's capacity. The control strategy can be applied to the drive systems whose

the converter's input phase voltage and current in motoring and regenerating mode. Fig. 13(d) shows the moment when the converter's input power factor changes from positive to negative.

Fig. 13(f) shows the converter's input and output power recorded by the central controller. The motor-generated power decreases as the motor speed decreases. The difference between these two power curves is about 180 W in which about 105 W is dissipated within the transformer and the rest is dissipated in the cells. Because the transformer was not designed for motor drive of such small power, the loss is relatively high. However, the converter's regeneration process can be observed, and all cells' dc-link voltages remain stable. Fig. 13(g) shows the angle β and the change of deceleration speed (df/dt) recorded by the central controller.

Fig. 14 shows the experimental result when the PWM rectifier control does not work and all cascaded cells output the same voltage. As the motor decelerates, the ordinary cell's dc-link voltage rapidly ramps to the threshold value of 120 V, causing the converter to shut down. When all cells' dc-link voltages ramp up, the converter's input current decreases to the no-load current of the phase-shift transformer.

These experimental results verify that the converter with the power tracking control strategy exactly delivers the regenerated power back to the grid and allows the motor to decelerate more quickly. The limitation of regenerated power sometimes is determined by the regenerative cell's capacity or the rated input current of the transformer's secondary windings, not the phase-shift angle limitation.

experimental results verify that, with the power tracking control strategy, this converter can deliver the motor-generated power back to the grid and all cells dc-link voltages remain stable.

References

[1] J. Lai and F. Z. Peng, "Multilevel converters—A new breed of power converters," *IEEE Trans. Ind. Appl.*, vol. 32, no. 3, pp. 509–517, May/Jun. 1996.

[2] S. Bernet, "Recent development of high power converters for industry and traction applications," *IEEE Trans. Power Electron.*, vol. 15, no. 6, pp. 1102–1117, Nov. 2000.

[3] J. Rodriguez, J. Lai, and F. Z. Peng, "Multilevel inverters: Survey of topologies, controls, and applications," *IEEE Trans. Ind. Appl.*, vol. 49, no. 4, pp. 724–738, Aug. 2002.

[4] R. Teodorescu, F. Blaabjerg, J. K. Pedersen, E. Cengelci, and P. N. Enjeti, "Multilevel inverter by cascading industrial VSI," *IEEE Trans. Ind. Electron.*, vol. 49, no. 4, pp. 832–838, Aug. 2002.

[5] B. Wu, "High-power converters and AC drives," in *Proc. IEEE PESC*, 2005, p. 416.

[6] J. Rodrıacute;guez, S. Bernet, B. Wu, J. Pontt, and S. Kouro, "Multilevel voltage-source-converter topologies for industrial medium-voltage drives," *IEEE Trans. Ind. Electron.*, vol. 54, no. 6, pp. 2930–2945, Dec. 2007.

[7] S. Kouro *et al.*, "Recent advances and industrial applications of multilevel converters," *IEEE Trans. Ind. Electron.*, vol. 57, no. 8, pp. 2553–2580, Aug. 2010.

[8] R. Ueda, T. Sonoda, K. Koga, and M. Ichikawa, "Stability analysis in induction motor driven by V/f controlled general-purpose inverter," *IEEE Trans. Ind. Appl.*, vol. 28, no. 2, pp. 472–481, Mar. 1992.

[9] A. Munoz-Garcia, T. A. Lipo, and D. W. Novotny, "A new induction motor V/f control method capable of high-performance regulation at low speeds," *IEEE Trans. Ind. Appl.*, vol. 34, no. 4, pp. 813–821, Jul./Aug. 1998.

[10] J. Jung, G. Jeong, and B. Kwon, "Stability improvement of V/f-controlled induction motor drive systems by a dynamic current compensator," *IEEE Trans. Ind. Electron.*, vol. 51, no. 4, pp. 930–933, Aug. 2004.

[11] M. Tsuji, S. Chen, S. Hamasaki, X. Zhao, and E. Yamada, "A novel V/f control of induction motors for wide and precise speed operation," in *Proc. Int. SPEEDAM*, 2008, pp. 1130–1135.
[12] X. Zhao, M. Tsuji, Y. Inaki, and S. Hamasaki, "Steady-State and transient characteristics of a novel V/f controlled induction motor," in *Proc. 15th ICEMS*, 2012, pp. 1–6.
[13] S. Islam, S. Ahmad, A. Iqbal, and F. I. Bakhsh, "Simplified stability analysis of a V/f controlled closed-loop induction motor drive System," in *Proc. IEEE 5th PICONF*, 2012, pp. 1–6.
[14] S. C. Agarlita, C. E. Coman, G. D. Andreescu, and I. Boldea, "Stable V/f control system with controlled power factor angle for permanent synchronous motor drives," *IET Elect. Power Appl.*, vol. 7, no. 4, pp. 278–286, Apr. 2013.
[15] J. Rodriguez, J. Pontt, E. Silva, J. Espinoza, and M. Perez, "Topologies for regenerative cascaded multilevel inverters," in *Proc. 34th IEEE PESC*, 2003, pp. 519–524.
[16] M. A. Perez, J. R. Espinoza, J. R. Rodriguez, and P. Lezana, "Regenerative medium-voltage AC drive based on a multicell arrangement with reduced energy storage requirements," *IEEE Trans. Ind. Electron.*, vol. 52, no. 1, pp. 171–180, Feb. 2005.
[17] J. Wang and Y. Li, "PWM rectifier in power cell of cascaded H-bridge multilevel converter," in *Proc. ICEMS*, 2007, pp. 18–21.
[18] B. Sun, J. Wang, and Y. Li, "PWM rectifier control for regenerative cascade inverter and its harmonic analysis," *Diangong Jishu Xuebao/Trans. China Electrotech. Soc.*, vol. 26, no. 7, pp. 210–215, Jul. 2011.
[19] J. Rodriguez *et al.*, "High-voltage multilevel converter with regeneration capability," *IEEE Trans. Ind. Electron.*, vol. 49, no. 4, pp. 839–846, Aug. 2002.
[20] P. Lezana, J. Rodriguez, D. Rojas, and J. Pontt, "Novel cell based on reduced single-phase active front end for multicell converters," in *Proc. 31st IEEE IECON*, 2005, pp. 733–738.
[21] J. R. Rodriguez, J. Dixon, J. Espinoza, J. Pontt, and P. Lezana, "PWM regenerative rectifiers: State of the art," *IEEE Trans. Ind. Electron.*, vol. 52,

Jinwu Gong received the B.Eng. and Ph.D. degrees in electrical engineering from Wuhan University, Wuhan, China, in 2004 and 2012, respectively.

He is currently a faculty member with the School of Electrical Engineering, Wuhan University. His research interests include high-power converters such as medium-voltage motor drives, static synchronous compensators, and active power filters.

Lan Xiong received the B.Eng. and M.Eng. degrees from Huazhong University of Science and Technology, Wuhan, China, in 2001 and 2004, respectively, and the Ph.D. degree from Wuhan University, Wuhan, China, in 2014, all in electrical engineering.

She is currently a faculty member with the School of Electrical and Electronic Engineering, Hubei University of Technology, Wuhan. Her research interests include cascaded multilevel converters and pulsewidth modulation techniques.

Fei Liu received the M.Eng. and Ph.D. degrees in electrical engineering from Huazhong University of Science and Technology, Wuhan, China, in 2004 and 2008, respectively.

He is currently an Associate Professor with the School of Electrical Engineering, Wuhan University, Wuhan. His research interests include renewable energy generation, distributed generation systems, dc microgrids, and cascaded multilevel converters.

[23] P. Lezana, J. Rodriguez, and D. A. Oyarzun, "Cascaded multilevel inverter with regeneration capability and reduced number of switches," *IEEE Trans. Ind. Electron.*, vol. 55, no. 3, pp. 1059–1066, Mar. 2008.
[24] K. Nagata, H. Nemoto, and T. Katayama, "An advanced multilevel inverter with a regenerative unit for motor drives," in *Proc. 13th EPE Conf. Appl.*, 2009, pp. 1–10.
[25] M. Rastog, R. H. Osman, and Y. Fukuta, "Variable-frequency drive with regeneration capability," U.S. Patent 7 508 147 B2, Mar. 24, 2009.
[26] L. Xiong, X. Zha, F. Liu, and J. Gong, "A regenerative cascaded multilevel converter with reduced active front ends," in *Proc. IEEE ECCE*, 2013, pp. 3491–3498.

Wuhan, China, in 1989, 1992 and 2001, respectively, all in electrical engineering.

Since 1992, he has been a faculty member with the School of Electrical Engineering, Wuhan University, where he is currently a Professor. From October 2001 to February 2003, he was a Postdoctoral Fellow with the University of Alberta, Edmonton, AB, Canada. His research interests include medium-voltage motor drives, apparatus for power quality control, static synchronous compensators, and application technologies of renewable energy resources in microgrid.